PHYSICAL REVIEW D **80,** 112003 (2009)

Higher-order multipole amplitudes in charmonium radiative transitions

M. Artuso,[1] S. Blusk,[1] S. Khalil,[1] R. Mountain,[1] K. Randrianarivony,[1] T. Skwarnicki,[1] S. Stone,[1] J. C. Wang,[1] L. M. Zhang,[1] G. Bonvicini,[2] D. Cinabro,[2] A. Lincoln,[2] M. J. Smith,[2] P. Zhou,[2] J. Zhu,[2] P. Naik,[3] J. Rademacker,[3] D. M. Asner,[4] K. W. Edwards,[4] J. Reed,[4] A. N. Robichaud,[4] G. Tatishvili,[4] E. J. White,[4] R. A. Briere,[5] H. Vogel,[5] P. U. E. Onyisi,[6] J. L. Rosner,[6] J. P. Alexander,[7] D. G. Cassel,[7] R. Ehrlich,[7] L. Fields,[7] R. S. Galik,[7] L. Gibbons,[7] S. W. Gray,[7] D. L. Hartill,[7] B. K. Heltsley,[7] J. M. Hunt,[7] D. L. Kreinick,[7] V. E. Kuznetsov,[7] J. Ledoux,[7] H. Mahlke-Krüger,[7] J. R. Patterson,[7] D. Peterson,[7] D. Riley,[7] A. Ryd,[7] A. J. Sadoff,[7] X. Shi,[7] S. Stroiney,[7] W. M. Sun,[7] J. Yelton,[8] P. Rubin,[9] N. Lowrey,[10] S. Mehrabyan,[10] M. Selen,[10] J. Wiss,[10] M. Kornicer,[11] R. E. Mitchell,[11] M. R. Shepherd,[11] C. M. Tarbert,[11] D. Besson,[12] T. K. Pedlar,[13] J. Xavier,[13] D. Cronin-Hennessy,[14] K. Y. Gao,[14] J. Hietala,[14] R. Poling,[14] P. Zweber,[14] S. Dobbs,[15] Z. Metreveli,[15] K. K. Seth,[15] B. J. Y. Tan,[15] A. Tomaradze,[15] S. Brisbane,[16] J. Libby,[16] L. Martin,[16] A. Powell,[16] P. Spradlin,[16] C. Thomas,[16] G. Wilkinson,[16] H. Mendez,[17] J. Y. Ge,[18] D. H. Miller,[18] I. P. J. Shipsey,[18] B. Xin,[18] G. S. Adams,[19] D. Hu,[19] B. Moziak,[19] J. Napolitano,[19] K. M. Ecklund,[20] J. Insler,[21] H. Muramatsu,[21] C. S. Park,[21] E. H. Thorndike,[21] and F. Yang[21]

(CLEO Collaboration)

[1]*Syracuse University, Syracuse, New York 13244, USA*
[2]*Wayne State University, Detroit, Michigan 48202, USA*
[3]*University of Bristol, Bristol BS8 1TL, UK*
[4]*Carleton University, Ottawa, Ontario, Canada K1S 5B6*
[5]*Carnegie Mellon University, Pittsburgh, Pennsylvania 15213, USA*
[6]*University of Chicago, Chicago, Illinois 60637, USA*
[7]*Cornell University, Ithaca, New York 14853, USA*
[8]*University of Florida, Gainesville, Florida 32611, USA*
[9]*George Mason University, Fairfax, Virginia 22030, USA*
[10]*University of Illinois, Urbana-Champaign, Illinois 61801, USA*
[11]*Indiana University, Bloomington, Indiana 47405, USA*
[12]*University of Kansas, Lawrence, Kansas 66045, USA*
[13]*Luther College, Decorah, Iowa 52101, USA*
[14]*University of Minnesota, Minneapolis, Minnesota 55455, USA*
[15]*Northwestern University, Evanston, Illinois 60208, USA*
[16]*University of Oxford, Oxford OX1 3RH, UK*
[17]*University of Puerto Rico, Mayaguez, Puerto Rico 00681*
[18]*Purdue University, West Lafayette, Indiana 47907, USA*
[19]*Rensselaer Polytechnic Institute, Troy, New York 12180, USA*
[20]*Rice University, Houston, Texas 77005, USA*
[21]*University of Rochester, Rochester, New York 14627, USA*
(Received 1 October 2009; published 28 December 2009)

Using 24×10^6 $\psi' \equiv \psi(2S)$ decays in CLEO-c, we have searched for higher multipole admixtures in electric-dipole-dominated radiative transitions in charmonia. We find good agreement between our data and theoretical predictions for magnetic quadrupole ($M2$) amplitudes in the transitions $\psi' \to \gamma\chi_{c1,c2}$ and $\chi_{c1,c2} \to \gamma J/\psi$, in striking contrast to some previous measurements. Let b_2^J and a_2^J denote the normalized $M2$ amplitudes in the respective aforementioned decays, where the superscript J refers to the angular momentum of the χ_{cJ}. By performing unbinned maximum likelihood fits to full five-parameter angular distributions, we found the following values of $M2$ admixtures for $J_\chi = 1$: $a_2^{J=1} = (-6.26 \pm 0.63 \pm 0.24) \times 10^{-2}$ and $b_2^{J=1} = (2.76 \pm 0.73 \pm 0.23) \times 10^{-2}$, which agree well with theoretical expectations for a vanishing anomalous magnetic moment of the charm quark. For $J_\chi = 2$, if we fix the electric octupole ($E3$) amplitudes to zero as theory predicts for transitions between charmonium S states and P states, we find $a_2^{J=2} = (-9.3 \pm 1.6 \pm 0.3) \times 10^{-2}$ and $b_2^{J=2} = (1.0 \pm 1.3 \pm 0.3) \times 10^{-2}$. If we allow for $E3$ amplitudes we find, with a four-parameter fit, $a_2^{J=2} = (-7.9 \pm 1.9 \pm 0.3) \times 10^{-2}$, $b_2^{J=2} = (0.2 \pm 1.4 \pm 0.4) \times 10^{-2}$, $a_3^{J=2} = (1.7 \pm 1.4 \pm 0.3) \times 10^{-2}$, and $b_3^{J=2} = (-0.8 \pm 1.2 \pm 0.2) \times 10^{-2}$. We determine the ratios $a_2^{J=1}/a_2^{J=2} = 0.67^{+0.19}_{-0.13}$ and $a_2^{J=1}/b_2^{J=1} = -2.27^{+0.57}_{-0.99}$, where the theoretical predictions are independent of the charmed quark magnetic moment and are $a_2^{J=1}/a_2^{J=2} = 0.676 \pm 0.071$ and $a_2^{J=1}/b_2^{J=1} = -2.27 \pm 0.16$.

DOI: 10.1103/PhysRevD.80.112003 PACS numbers: 13.20.Gd, 13.40.Em, 13.40.Hq, 14.40.Gx

I. INTRODUCTION

The radiative transitions between spin-triplet charmonium states are known to be dominated by electric dipole ($E1$) amplitudes, but higher multipole contributions, magnetic quadrupole and electric octupole ($M2$ and $E3$), are sometimes allowed. These higher multipoles give information about the magnetic moment of the charm quark. To search for these contributions, we studied the radiative decay sequences

$$e^+e^- \to \gamma^* \to \psi' \equiv \psi(2S) \qquad \psi' \to \gamma'\chi_{(c1,c2)}$$
$$\chi_{(c1,c2)} \to \gamma J/\psi \qquad J/\psi \to e^+e^- \quad \text{or} \quad \mu^+\mu^-$$

using the helicity formalism developed in Refs. [1–4]. As shown in Fig. 1, the particles ψ', $\chi_{(c1,c2)}$, and J/ψ are the $2\,^3S_1$, $1\,^3P_{(1,2)}$, and $1\,^3S_1$ charmonium states, respectively. For the $J_\chi = 1$ decay sequence, we search for two multipole amplitudes, $b_2^{J=1}$ and $a_2^{J=1}$, which are, respectively, the $M2$ amplitudes for the $\psi' \to \gamma'\chi_{c1}$ (b for before the χ_c) and $\chi_{c1} \to \gamma J/\psi$ decay (a for after the χ_c). Similarly, for the $J_\chi = 2$ decay sequence, we search for two $M2$ amplitudes ($b_2^{J=2}$, $a_2^{J=2}$) and two $E3$ amplitudes ($b_3^{J=2}$, $a_3^{J=2}$).

The multipole amplitudes are calculated from a maximum likelihood fit of the joint angular distribution of the two photons γ' and γ, described by five angles for each event. Polar and azimuthal angles (θ', ϕ') denote the direction of the initial e^+e^- axis relative to the first photon γ' (in the ψ' frame), an angle $\theta_{\gamma\gamma'}$ describes the direction between the two photons (in the χ_c frame), and polar and azimuthal angles (θ, ϕ) denote the direction of the final lepton pair ($\ell^+\ell^-$) axis relative to the second photon γ (in the J/ψ frame). These angles are illustrated in Fig. 2.

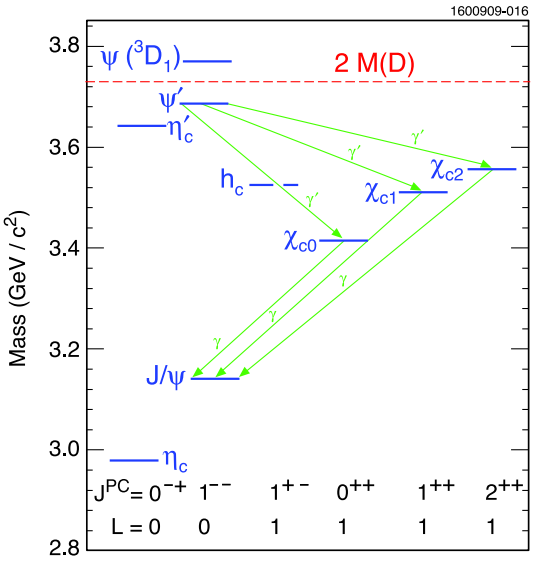

FIG. 1 (color online). Charmonium energy levels. Only the transitions studied in this article are shown.

In previous experimental studies of $\chi_{cJ} \to \gamma J/\psi$, the magnetic quadrupole amplitude in the decay sequences involving χ_{c1} was found to be consistent with zero, while that found via χ_{c2} was found to be several standard deviations from zero. However, theory predicts the ratio of these two magnetic quadrupole amplitudes to be of order unity. With CLEO's large sample of ψ' decays, the question is ripe for reinvestigation. The present paper describes that effort.

Section II sets the theoretical stage for the investigation. Prior experimental results are reviewed in Sec. III. The CLEO detector, data sets, and Monte Carlo samples are described in Sec. IV. Section V discusses selection criteria, while Sec. VI is devoted to fits to the data. Systematic uncertainties are treated in Sec. VII, while Sec. VIII concludes.

II. THEORETICAL CONTEXT

A. Allowed radiative transitions

For the radiative decays between a $^3S_1$ state and a $^3P_1$ state, only $E1$ and $M2$ transitions are allowed. For $^3S_1 \to {}^3P_2$ transitions, from conservation of angular momentum and parity, we would expect that the $E3$ transition would be allowed, but this is forbidden under the single-quark radiation hypothesis [2,5]. Single-quark radiative transitions must have $|\Delta S| \leq 1$ and parity-changing transitions must have $|\Delta L| = 1$, so the photon cannot carry off three units of angular momentum [1]. However, for the $J_\chi = 2$ case, electric octupole transitions are allowed if either S state has a small D admixture [6], or if the P state has a small F admixture. There is evidence [6–8] that the ψ' state is

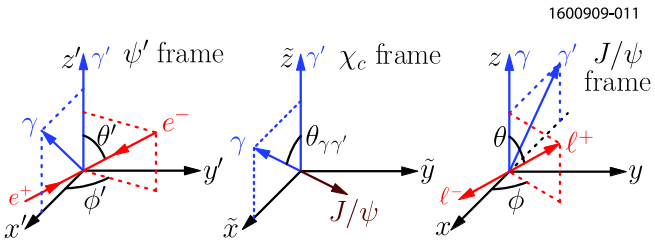

FIG. 2 (color online). Reference frames defining the angles used in this analysis. In the ψ' frame, the angles θ', ϕ' are the polar and azimuthal angles of the beam pipe (specifically, the positron's direction) relative to γ' defining the z' axis, and γ lying in the x'-z' plane (with a *positive* x' component). In the χ_c frame, the angle $\theta_{\gamma\gamma'}$ is the angle between the two photons. In the J/ψ frame, the angles θ, ϕ are the polar and azimuthal angles of the two leptons (specifically, the positive lepton's direction) relative to γ defining the z axis, and γ' lying in the x-z plane (with a *negative* x component).

actually a mixture $\cos\varphi|2\,^3S_1\rangle - \sin\varphi|^3D_1\rangle$ with $\varphi = (12 \pm 2)°$, so we may expect a small b_3 transition amplitude.

B. Joint angular distribution

The formalism developed in Refs. [1,2,9] is used to construct the joint angular distribution of the decay sequence. We denote the signal decay as

$$\psi'(\lambda') \to \gamma'(\mu') + \chi(\nu'), \tag{1}$$

$$\chi(\nu) \to \gamma(\mu) + J/\psi(\lambda), \tag{2}$$

with helicities in parentheses and the helicities associated with the ψ' decay labeled with primes. For the ψ' (χ_c) decay sequence, the helicity amplitudes are labeled $B_{\nu'}$ (A_ν) and the multipole amplitudes are labeled b_{J_γ} ($a_{J_{\gamma'}}$), where J_γ is the angular momentum carried by the photon γ. The helicity amplitudes are specified by only one helicity, since parity conservation allows the independent helicity amplitudes to be defined for $J_\chi \geq \nu \geq 0$ as

$$B_{\nu'} \equiv B_{\nu',1} = (-1)^{J_\chi} B_{-\nu',-1},$$
$$A_\nu \equiv A_{\nu,1} = (-1)^{J_\chi} A_{-\nu,-1}.$$

Here, the second index of the two-index helicities refers to the photon. To form the joint angular distribution the ψ' and J/ψ density matrices must be constructed from the directions of the two electrons forming the ψ' and the two leptons that decay from the J/ψ.[1]

The angles θ', ϕ' contain information on the polarization of the ψ', while θ, ϕ contain information on the polarization of the J/ψ. The angle $\theta_{\gamma\gamma'}$, defined by the angle between the two photons in the χ_c rest frame, gives information on the necessary rotation between the two reference frames. Frames for construction of these five angles have been shown above in Fig. 2. The joint angular distribution is therefore

$$W(\cos\theta', \phi', \cos\theta_{\gamma\gamma'}, \cos\theta, \phi) \propto \sum_{\substack{\nu'\tilde{\nu}';\mu'=\pm1 \\ \tilde{\nu}\nu;\mu=\pm1}} \rho^{(\mu'-\nu',\mu'-\tilde{\nu}')}(\theta', \phi') B_{|\nu'|} B_{|\tilde{\nu}'|} d^{J_\chi}_{-\nu'\nu}(\theta_{\gamma\gamma'}) \times d^{J_\chi}_{-\tilde{\nu}'\tilde{\nu}}(\theta_{\gamma\gamma'}) A_{|\nu|} A_{|\tilde{\nu}|} \rho^{*(\nu-\mu,\tilde{\nu}-\mu)}(\theta, \phi), \tag{3}$$

where $d^{J_\chi}_{\nu'\nu}$ are standard Wigner d functions [10].

The helicity amplitudes A_ν (with $0 \leq \nu \leq J_\chi$) are related to the multipole amplitudes a_{J_γ} (with $1 \leq J_\gamma \leq J_\chi + 1$), using the Clebsch-Gordan coefficients $\langle j_1, m_1; j_2, m_2 | J, M\rangle$, by

$$A^{J_\chi}_\nu = \sum_{J_\gamma} \sqrt{\frac{2J_\gamma + 1}{2J_\chi + 1}}\, a^{J_\chi}_{J_\gamma} \langle J_\gamma, 1; 1, \nu - 1 | J_\chi, \nu\rangle. \tag{4}$$

This expression leads to the following relationships for the $J_\chi = 1$ and $J_\chi = 2$ cases, respectively,

$$\begin{pmatrix} A^{J=1}_0 \\ A^{J=1}_1 \end{pmatrix} = \begin{pmatrix} \sqrt{\frac{1}{2}} & \sqrt{\frac{1}{2}} \\ \sqrt{\frac{1}{2}} & -\sqrt{\frac{1}{2}} \end{pmatrix} \begin{pmatrix} a^{J=1}_1 \\ a^{J=1}_2 \end{pmatrix}, \tag{5}$$

$$\begin{pmatrix} A^{J=2}_0 \\ A^{J=2}_1 \\ A^{J=2}_2 \end{pmatrix} = \begin{pmatrix} \sqrt{\frac{1}{10}} & \sqrt{\frac{1}{2}} & \sqrt{\frac{2}{5}} \\ \sqrt{\frac{3}{10}} & \sqrt{\frac{1}{6}} & -\sqrt{\frac{8}{15}} \\ \sqrt{\frac{3}{5}} & -\sqrt{\frac{1}{3}} & \sqrt{\frac{1}{15}} \end{pmatrix} \begin{pmatrix} a^{J=2}_1 \\ a^{J=2}_2 \\ a^{J=2}_3 \end{pmatrix}. \tag{6}$$

The relationships between $B_{\nu'}$ and $b_{J_{\gamma'}}$ are identical; just swap all A_ν and a_{J_γ} with $B_{\nu'}$ and $b_{J_{\gamma'}}$ in Eqs. (4)–(6). These transformation matrices are norm-preserving, since the matrices are orthogonal.

C. Quark magnetic moments

If we define $E1$, $M2$, and $E3$ to be the electric dipole, magnetic quadrupole, and electric octupole amplitudes, respectively, the magnetic quadrupole amplitudes are related to the anomalous magnetic moment of the charm quark κ_c by

$$a^{J=1}_2 \equiv \frac{M2}{\sqrt{E1^2 + M2^2}} = -\frac{E_\gamma}{4m_c}(1 + \kappa_c), \tag{7}$$

$$a^{J=2}_2 \equiv \frac{M2}{\sqrt{E1^2 + M2^2 + E3^2}} = -\frac{3}{\sqrt{5}}\frac{E_\gamma}{4m_c}(1 + \kappa_c), \tag{8}$$

$$b^{J=1}_2 \equiv \frac{M2}{\sqrt{E1^2 + M2^2}} = \frac{E_{\gamma'}}{4m_c}(1 + \kappa_c), \tag{9}$$

$$b^{J=2}_2 \equiv \frac{M2}{\sqrt{E1^2 + M2^2 + E3^2}} = \frac{3}{\sqrt{5}}\frac{E_{\gamma'}}{4m_c}(1 + \kappa_c). \tag{10}$$

These expressions are correct to first order in E_γ/m_c or $E_{\gamma'}/m_c$, assuming that the $\psi(1S, 2S)$ are pure S states (no

[1] In $e^+e^- \to \gamma^* \to \psi'$, the polarization of the ψ' along the beam axis is ± 1, so the density matrix giving the polarizations in the direction of the beam axis (the z axis) is given by $\rho^{(\lambda'\tilde{\lambda}')} = \epsilon_1^{*(\lambda')}\epsilon_1^{(\tilde{\lambda}')} + \epsilon_2^{*(\lambda')}\epsilon_2^{(\tilde{\lambda}')}$, where $\epsilon^{(\lambda)}$ is the polarization vector for helicity λ defined with components $\epsilon^{(1)} = (-1, -i, 0)/\sqrt{2}$, $\epsilon^{(0)} = (0, 0, 1)$ and $\epsilon^{(-1)} = -\epsilon^{(1)*} = (1, -i, 0)/\sqrt{2}$. Generalizing to an arbitrary direction $\hat{n} \equiv (\sin\theta'\cos\phi', \sin\theta'\sin\phi', \cos\theta')$, we find that the density matrix ρ for ψ' is

$$\rho^{(\lambda',\tilde{\lambda}')}(\theta', \phi') = \sum_{i,j} \epsilon_i^{*(\lambda')}\epsilon_j^{(\tilde{\lambda}')}(\delta^{ij} - n^i n^j).$$

Similarly, for the J/ψ with $\hat{m} \equiv (\sin\theta\cos\phi, \sin\theta\sin\phi, \cos\theta)$, we find the density matrix is

$$\rho^{(\lambda,\tilde{\lambda})}(\theta, \phi) = \sum_{i,j} \epsilon_i^{*(\lambda)}\epsilon_j^{(\tilde{\lambda})}(\delta^{ij} - m^i m^j).$$

mixing with D states) and that the χ_c states are pure P states (no mixing with F states) [3,11].[2]

These first order relationships are derived from the nonrelativistic interaction Hamiltonian for photon emission from a $+2/3$ charged quark:

$$H_I = -\frac{e_c}{2m_c}(\mathbf{A}^* \cdot \mathbf{p} + \mathbf{p} \cdot \mathbf{A}^*) - \mu\sigma \cdot \mathbf{H}^*, \qquad (11)$$

where $e_c \equiv \frac{2}{3}|e|$, $\mu \equiv (e_c/2m_c)(1 + \kappa_c)$, $\mathbf{A}^*$ is the vector potential of the emitted photon, and $\mathbf{H}^* \equiv \nabla \times \mathbf{A}^*$ is the magnetic field of the emitted photon (both $\mathbf{A}^*$ and $\mathbf{H}^*$ are complex conjugated since the photon is outgoing). We omit a spin-orbit term of the same order, which does not affect the $M2$ contribution [2,13].

The ratios of the predicted multipole amplitudes given by Eqs. (7)–(10) are independent of m_c and κ_c to first order:

$$\left(\frac{a_2^{J=1}}{a_2^{J=2}}\right)_{\text{th}} = \frac{E_\gamma^{J=1}}{E_\gamma^{J=2}}\frac{\sqrt{5}}{3} = 0.676 \pm 0.071, \qquad (12)$$

$$\left(\frac{a_2^{J=1}}{b_2^{J=1}}\right)_{\text{th}} = -\frac{E_\gamma^{J=1}}{E_{\gamma'}^{J=1}} = -2.27 \pm 0.16, \qquad (13)$$

$$\left(\frac{b_2^{J=2}}{b_2^{J=1}}\right)_{\text{th}} = \frac{E_{\gamma'}^{J=2}}{E_{\gamma'}^{J=1}}\frac{3}{\sqrt{5}} = 1.000 \pm 0.015, \qquad (14)$$

$$\left(\frac{b_2^{J=2}}{a_2^{J=2}}\right)_{\text{th}} = -\frac{E_{\gamma'}^{J=2}}{E_\gamma^{J=2}} = -0.297 \pm 0.025. \qquad (15)$$

As the individual amplitudes have corrections of order $(E_\gamma/m_c)^2$, we conservatively assigned each multipole amplitude a fractional uncertainty equal to $(E_\gamma/m_c)^2$ (using $m_c = 1.5$ GeV, $\kappa_c = 0$) which was the dominant source of uncertainty in Eqs. (12)–(15).

The $E3$ amplitudes are expected to be small in view of the few-percent admixture of the $1\,^3D_1$ state in the ψ'. Although they are found to be complex in Ref. [11], we shall include them in fits assuming that they are real.

D. Lattice QCD predictions

Dudek *et al.* [14,15] performed lattice QCD calculations for the charmonium radiative transitions $\chi_{(c1,c2)} \to \gamma J/\psi$. They ran lattice simulations at various values of Q^2 (the square of the four-vector of the photon, which is 0 for real photons) and extrapolated to $Q^2 \to 0$.

For the transition $\chi_{c1} \to \gamma J/\psi$, when extrapolating the $E1$ and $M2$ amplitudes to $Q^2 \to 0$ individually, they found that

$$\frac{M2(Q^2 \to 0)}{E1(Q^2 \to 0)} = \frac{-0.020 \pm 0.017}{0.23 \pm 0.03} = -0.09 \pm 0.07. \qquad (16)$$

They concluded that data points at smaller Q^2 and improved knowledge of form factors were needed to make a meaningful comparison with experimental values [15]. Similarly, for $\chi_{c2} \to \gamma J/\psi$, they found the normalized multipole amplitudes behaving as $a_2^{J=2} \to -0.39 \pm 0.07$, $a_3^{J=2} \to 0.010 \pm 0.011$ as $Q^2 \to 0$.

III. PRIOR EXPERIMENTAL RESULTS

Tables I and II summarize the results from previous experiments for $J_\chi = 1$ and $J_\chi = 2$, respectively.

For transitions involving χ_{c1}, the Crystal Ball experiment at SPEAR used 921 events of $e^+e^- \to \psi' \to \gamma'\chi_{c1} \to \gamma'\gamma J/\psi \to \gamma'\gamma\ell^+\ell^-$ to measure both multipole amplitudes. The E-835 experiment used 2090 $p\bar{p} \to \chi_{c1} \to \gamma J/\psi \to \gamma e^+e^-$ events to measure the multipole amplitude $a_2^{J=1}$. The CLEO-c data sample has $\simeq 40\,000$ $e^+e^- \to \psi' \to \gamma'\chi_{c1} \to \gamma'\gamma J/\psi \to \gamma'\gamma\ell^+\ell^-$ events after applying selection criteria.

For transitions involving χ_{c2}, the Crystal Ball experiment used 441 events of $e^+e^- \to \psi' \to \gamma'\chi_{c2} \to \gamma'\gamma J/\psi \to \gamma\gamma'\ell^+\ell^-$ to measure both multipole amplitudes. The E-760 and E-835 experiments used 1904 and 5908 $p\bar{p} \to \chi_{c2} \to \gamma J/\psi \to \gamma e^+e^-$ events, respectively, to measure the multipole amplitude $a_2^{J=2}$. The BESII experiment searched for the multipole amplitudes in a novel method looking at 418 $\psi' \to \gamma\chi_{c2} \to \gamma\pi^+\pi^-$ events and 303 $\psi' \to \gamma\chi_{c2} \to \gamma K^+K^-$ events, and the BESII fit also found a value of $b_3^{J=2} = -0.027^{+0.043}_{-0.029}$. The CLEO-c data sample has $\simeq 20\,000$ $e^+e^- \to \psi' \to \gamma'\chi_{c2} \to \gamma'\gamma J/\psi \to \gamma'\gamma\ell^+\ell^-$ events after applying selection criteria.

Many of these experimental results disagreed with the theory that predicted the ratios given in Eqs. (12)–(15). The ratios of the averages of previous experimental values compared with theory values are

TABLE I. Previous experimental values vs theoretical predictions for the normalized magnetic quadrupole amplitude for the decays $\chi_{c1} \to \gamma J/\psi$ ($a_2^{J=1}$) and $\psi' \to \gamma'\chi_{c1}$ ($b_2^{J=1}$).

Experiment	$a_2^{J=1}$	$b_2^{J=1}$	Signal Events
Crystal Ball [16,17]	$-0.002^{+0.008}_{-0.020}$	$0.077^{+0.050}_{-0.045}$	921
E-835 [12]	$0.002 \pm 0.032 \pm 0.004$		2090
Theory ($m_c = 1.5$ GeV)	$-0.065(1 + \kappa_c)$	$0.029(1 + \kappa_c)$	

TABLE II. Previous experimental values vs theoretical predictions for the normalized magnetic quadrupole amplitudes for the decays $\chi_{c2} \to \gamma J/\psi$ ($a_2^{J=2}$) and $\psi' \to \gamma' \chi_{c2}$ ($b_2^{J=2}$).

Experiment	$a_2^{J=2}$	$b_2^{J=2}$	Signal Events
Crystal Ball [16,17]	$-0.333^{+0.116}_{-0.292}$	$0.132^{+0.098}_{-0.075}$	441
E-760 [18]	-0.14 ± 0.06		1904
E-835 [12]	$-0.093^{+0.039}_{-0.041} \pm 0.006$		5908
BESII [19]		$-0.051^{+0.054}_{-0.036}$	731
Theory ($m_c = 1.5$ GeV)	$-0.096(1 + \kappa_c)$	$0.029(1 + \kappa_c)$	

$$\left(\frac{a_2^{J=1}}{a_2^{J=2}}\right)_{\rm exp} = \frac{-0.002 \pm 0.020}{-0.13 \pm 0.05} = 0.02^{+0.17}_{-0.16} \stackrel{?}{=} \left(\frac{a_2^{J=1}}{a_2^{J=2}}\right)_{\rm th} = 0.676 \pm 0.071, \quad (17)$$

$$\left(\frac{a_2^{J=1}}{b_2^{J=1}}\right)_{\rm exp} = \frac{-0.002 \pm 0.020}{0.077 \pm 0.050} = -0.02^{+0.30}_{-0.32} \stackrel{?}{=} \left(\frac{a_2^{J=1}}{b_2^{J=1}}\right)_{\rm th} = -2.27 \pm 0.16, \quad (18)$$

$$\left(\frac{b_2^{J=2}}{b_2^{J=1}}\right)_{\rm exp} = \frac{0.132 \pm 0.075}{0.077 \pm 0.050} = 1.5^{+2.2}_{-1.1} \stackrel{?}{=} \left(\frac{b_2^{J=2}}{b_2^{J=1}}\right)_{\rm th} = 1.000 \pm 0.015, \quad (19)$$

$$\left(\frac{b_2^{J=2}}{a_2^{J=2}}\right)_{\rm exp} = \frac{0.132 \pm 0.075}{-0.13 \pm 0.05} = -1.01^{+0.60}_{-0.93} \stackrel{?}{=} \left(\frac{b_2^{J=2}}{a_2^{J=2}}\right)_{\rm th} = -0.297 \pm 0.025. \quad (20)$$

The first two ratios, which involve the multipole amplitudes that have the most statistical significance, strongly disagree with their theoretical predictions. As the ratios are independent of m_c, κ_c and any specific quarkonium potential model to first order in $E_\gamma/(4m_c)$, we expect good agreement between theory and experiment.

IV. DETECTOR, DATA, AND MONTE CARLO

A. The CLEO detector

Data were acquired at the ψ' resonance at $\sqrt{s} = 3.686$ GeV using the CLEO-c detector located at the Cornell Electron Storage Ring (CESR), a symmetrical e^+e^- collider [20,21]. The solid angle for detecting both charged and neutral particles is 93% of 4π. The photons were detected as showers in a CsI (Tl) calorimeter consisting of 7784 crystals, which achieved a photon energy resolution of 2.2% at 1 GeV and 5% at 100 MeV. The azimuthal and polar angular resolution for 100 MeV photons is $\sigma_{\phi_{\rm azim}} \approx 11$ mrad (19 mrad) and $\sigma_{\theta_{\rm polar}} \approx 0.8\sigma_{\phi_{\rm azim}} \sin\theta_{\rm polar}$ (10 mrad) in the barrel (endcap) region of the crystal calorimeter. Charged particles were detected using a set of two cylindrical drift chambers enclosed within a superconducting solenoid with a 1.0 T magnetic field directed along the beam axis. The outer drift chamber achieved a momentum resolution of $\approx 0.6\%$ at $p = 1$ GeV and an azimuthal and polar angular resolution of $\sigma_{\phi_{\rm azim}} \approx 1$ mrad and $\sigma_{\theta_{\rm polar}} \approx 4$ mrad [20]. (In this paper, $c = 1$ in mass and momentum units.) The inner six-layer stereo drift chamber is used to accurately measure the location of charged particles along the beam axis.

B. Data sets and expected number of events

For our analysis, we used the recent CLEO-c data set taken at the ψ' events consisting of a sample of $(24.45 \pm 0.49) \times 10^6$ ψ' events with a total luminosity of 48.07/pb [22]. Using known branching fractions [10] and the known sizes of the CLEO data sample, we can expect that $91\,900 \pm 6600$ $J_\chi = 1$ signal events and $48\,200 \pm 3600$ $J_\chi = 2$ signal events are originally present in the data sample.

C. Phase space Monte Carlo

For each of the decay sequences ($J_\chi = 1$ and $J_\chi = 2$), a 4.5×10^6 event phase space Monte Carlo (MC) data sample was generated. The phase space MC was generated with EVTGEN [23] with final state radiation simulated with PHOTOS [24].

The purposes of the phase space Monte Carlo are threefold. First, it is used to account for the variable angular efficiency of the detector after selection criteria have been applied, when performing the maximum likelihood fit (see Sec. VI A). Second, the phase space MC events are used to simulate signal MC with nonzero multipole amplitudes, a_2, b_2 (and a_3, b_3 for $J_\chi = 2$) via the rejection method. This is achieved by taking the five angles θ', ϕ', $\theta_{\gamma\gamma'}$, θ, ϕ for each phase space event and calculating the probability of that event occurring at those angles for the probability distribution function (PDF) $W(\Omega; \mathcal{A}_0)$ with the input values of the multipole amplitudes $\mathcal{A}_0$. The probability for the event occurring at that angle is then compared to a

[2]Note the misprint in [11] for their Eq. (41) describing $a_2^{J=2}$ to first order. This misprint was previously noted in footnote 1 of Ref. [12].

random number uniformly distributed between 0 and 1. Then, our simulated signal MC obeying the PDF $W(\Omega; \mathcal{A}_0)$ consists of the events that are more probable than the corresponding random numbers. The third purpose of the phase space Monte Carlo is to generate projections to overlay upon histograms of data values. For example, after a fit to data extracts values of a_2, b_2 for a $J_\chi = 1$ fit, the phase space MC can be used to generate projections in the five angles with the fitted values of a_2, b_2 to be compared with the data.

D. Generic Monte Carlo

In order to properly simulate feed-across into the selected data sample from nonsignal ψ' decays, a "generic" MC sample was prepared. This sample consists of approximately 120×10^6 ψ' decays, using our best estimate for all measured branching fractions [10,22,25–33] and matrix elements for the decays of ψ' and its decay products; unmeasured hadronic decays are simulated using JETSET [34]. The signal events ($\psi' \to \gamma' \chi_{(c1,c2)} \to \gamma' \gamma J/\psi$) were replaced with phase space MC events selected to have the desired a_2 and b_2 admixture (via the rejection method as described in Sec. IV C).

V. SELECTION CRITERIA

Tuning of the selection criteria was designed to eliminate nonsignal "impure" background events, while selecting the largest number of signal events. For kinematic regions in which it was uncertain how to apply selection criteria, we attempted to minimize the quadrature sum of the statistical uncertainty from signal events and the systematic uncertainty from impure events. Many of the starting points for our selection criteria are taken from a CLEO-c study [22] of $\psi' \to h + J/\psi$ branching fractions that included our signal decays.

All tracks and showers investigated are required to pass standard CLEO-c criteria prior to any attempts at kinematic fitting. For tracks, we ensure that the track originated from near the interaction point ($r_0 < 2$ cm and $|z_0 - z_{\text{i.p.}}| < 10$ cm), is from the well-modeled region of the barrel ($|\cos\theta_{\text{polar}}| < 0.83$) or the endcap ($0.85 < |\cos\theta_{\text{polar}}| < 0.93$), and has a momentum between 1% (18.4 MeV/c) and 120% (2.21 GeV/c) of the beam momentum. The requirement for a shower is that it is not matched to a track, has $|\cos\theta_{\text{polar}}| < 0.79$ or $0.85 < |\cos\theta_{\text{polar}}| < 0.93$, and has an energy between 1% and 120% of the beam energy.

All candidate events require at least two tracks and two showers to be identified. The two tracks and two showers used (if more are present) will be those with the greatest energies. Two kinematic fits are then performed to generate the four 4-vectors used in the analysis. First, a 1C kinematic fit to the J/ψ mass is performed starting with the two tracks, allowing shower(s) identified as bremsstrahlung photons to be associated with a track. Bremsstrahlung photons are identified if a shower that is not matched to a track is located within 100 mrad of the initial momentum vector of a track. If bremsstrahlung photons are identified, the lepton four-vector used is the sum of the kinematically fit 4-vectors of the lepton plus all associated bremsstrahlung photons. Second, a 4C kinematic fit to the ψ' 4-vector is performed and the result of this fit is then subjected once more to the original 1C fit. The ψ' 4-vector is calculated from the angle at which the electron and positron beams intersect (4 mrad) and the beam energy of the given run. For both the 1C and 4C kinematic fits, we require the reduced χ^2 for both the vertex and kinematic fit to be less than 16 as shown in Fig. 3. This value was found by minimizing the quadrature sum of the impurity systematic uncertainty and statistical uncertainty.

To identify signal events through the J_χ radiative cascade, we require the reconstructed χ_{cJ} mass to be within 15 MeV of the true χ_{cJ} mass as constructed by adding the J/ψ and γ four-vectors together:

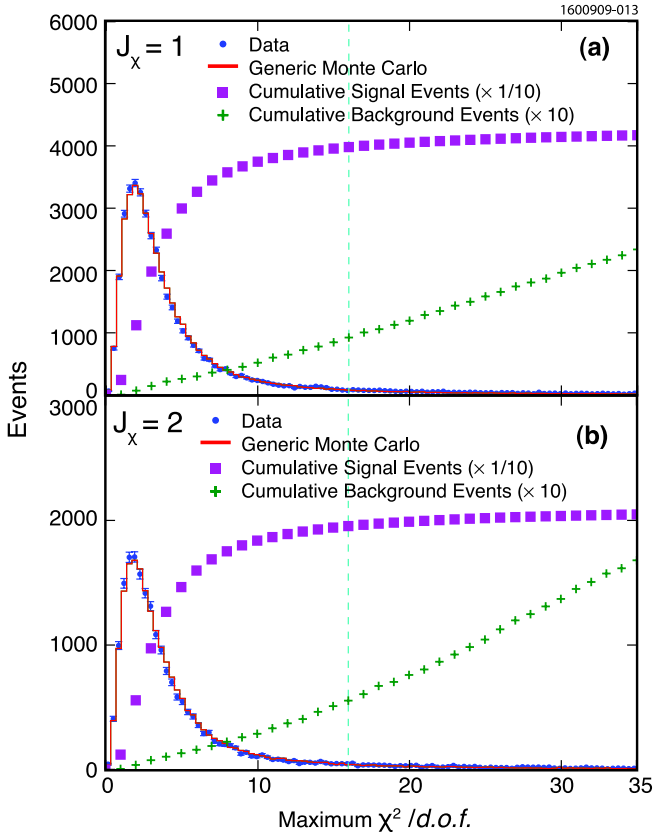

FIG. 3 (color online). Maximum reduced χ^2 in all kinematic fits (including vertex fits) in generic Monte Carlo and data. Events with a maximum reduced χ^2 below 16 (the dashed vertical line) are kept. Cumulative totals for the number of signal and impurity background events are also plotted for each potential value of a maximum reduced χ^2. (a) $J_\chi = 1$ and (b) $J_\chi = 2$.

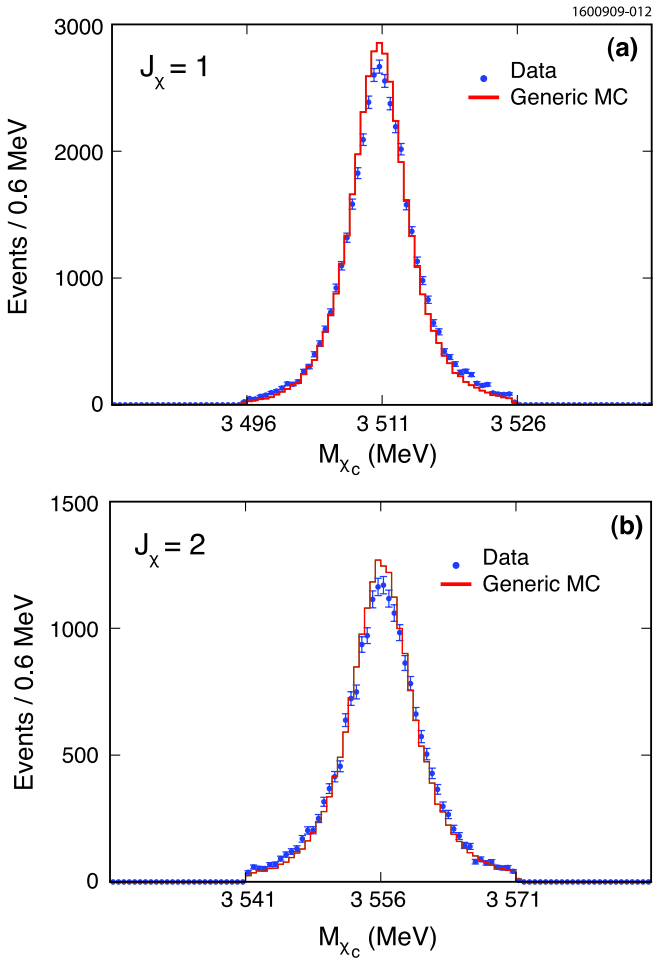

FIG. 4 (color online). Plot of the χ_{cJ} mass as calculated from subtracting the four-vector of the γ' from the ψ' four-vector. This variable is not used as a selection criterion because the 1C and 4C kinematic fits ensure that this criterion is redundant with the χ_{c1} mass selection criterion generated by adding the J/ψ and γ four-vectors. (a) $J_\chi = 1$ and (b) $J_\chi = 2$.

$$m_{\chi_{cJ}} = \sqrt{|p_{J/\psi} + p_\gamma|^2} = \sqrt{|p_{\ell^+} + p_{\ell^-} + p_\gamma|^2}. \quad (21)$$

We do not apply a selection criterion based on the other χ_{cJ} mass reconstructed from the ψ' and γ', as the 4C kinematic fit ensures that this criterion is redundant (see Fig. 4).

Signal events must also have the J/ψ decay to e^+e^- or $\mu^+\mu^-$, so we require the two tracks to be well identified as both being electrons or muons. We achieve this by looking at the ratio of the energy deposited in the calorimeter to the momentum of the track (E/p). We identify both tracks as electrons if the smaller E/p ratio is greater than 0.5 and the larger E/p ratio is greater than 0.85. Similarly, we identify both tracks as muons if $(E/p)_{\rm smaller} < 0.25$ and $(E/p)_{\rm larger} < 0.5$. This results in a clean $e - \mu$ separation.

To restrict major sources of background, we apply additional criteria to address the modes with large branching fractions:

$$\mathcal{B}(\psi' \to \pi^0\pi^0 J/\psi) = (16.84 \pm 0.33)\%$$
$$\mathcal{B}(\psi' \to \eta J/\psi) = (3.16 \pm 0.07)\%$$
$$\mathcal{B}(\psi' \to \pi^0 J/\psi) = (1.26 \pm 0.13) \times 10^{-3}. \quad (22)$$

The dominant background mode $\psi' \to \pi^0\pi^0 J/\psi \to \gamma\gamma\gamma\gamma\ell^+\ell^-$ is reduced by requiring the third most energetic shower in the event (excluding those photons identified as bremsstrahlung photons) to have an energy of less than 30 MeV. To reduce the contributions of the background modes with monochromatic J/ψ momentum, $\psi' \to \eta J/\psi \to \gamma\gamma J/\psi$ and $\psi' \to \pi^0 J/\psi \to \gamma\gamma J/\psi$ where $p(J/\psi)|_{\psi' \to \eta J/\psi} = 199\,\text{MeV}$ and $p(J/\psi)|_{\psi' \to \pi^0 J/\psi} = 528\,\text{MeV}$, we require the J/ψ momentum to lie between 240 MeV and 510 MeV. Note that the signal transition generates no events with a J/ψ momentum below 238 MeV (318 MeV for $J_\chi = 2$) or above 542 MeV.

VI. FITTING THE DATA

A. Basic approach and procedure

We find the multipole amplitudes by performing a maximum likelihood fit of the selected data events to the PDF $W(\Omega; \mathcal{A})$ given by Eq. (3). Events are selected according to the criteria described in Sec. V, and each event is described by a set of five angles $\Omega \equiv (\theta', \phi', \theta_{\gamma\gamma}, \theta, \phi)$ defined in Fig. 2. The PDF $W(\Omega; \mathcal{A})$ gives the probability for an event with angles Ω to occur given a set of multipole amplitudes $\mathcal{A} \equiv (a_i, b_j)$. The PDF in Eq. (3) is written in terms of helicity amplitudes, but can be written in terms of multipole amplitudes as $W(\Omega; \mathcal{A})$ using Eq. (4). The total likelihood for N_d data events to be described by $W(\Omega; \mathcal{A})$ is

$$\mathcal{L}_W(\mathcal{A}) \equiv \prod_{d=1}^{N_d} W(\Omega_d; \mathcal{A}). \quad (23)$$

The initially unknown angular detector efficiency $\epsilon(\Omega)$ describes the probability that an event occurring at the angles Ω will be registered by the detector and pass the selection criteria. We define a new normalized PDF to account for this detector efficiency $\epsilon(\Omega)$:

$$F(\Omega; \mathcal{A}) \equiv \frac{\epsilon(\Omega) W(\Omega; \mathcal{A})}{\int \epsilon(\Omega') W(\Omega'; \mathcal{A}) d\Omega'} \quad (24)$$

and note that the original PDF $W(\Omega; \mathcal{A})$ is of the form

$$W(\Omega; \mathcal{A}) = \sum_{ijkl} a_i a_j b_k b_l G_{ijkl}(\Omega). \quad (25)$$

The functions $G_{ijkl}(\Omega)$ are obtained from the expression for $W(\Omega; \mathcal{A})$, so this form allows separation of the parameters being determined (the multipole amplitudes $\mathcal{A}$) and the data points (the angles Ω). This allows us to write the denominator of the PDF in Eq. (24) as

$$\int \epsilon(\Omega')W(\Omega';\mathcal{A})d\Omega' = \int \epsilon(\Omega')\sum_{ijkl} a_i a_j b_k b_l G_{ijkl}(\Omega')d\Omega'$$
$$= \sum_{ijkl} a_i a_j b_k b_l \int \epsilon(\Omega')G_{ijkl}(\Omega')d\Omega'$$
$$= \sum_{ijkl} a_i a_j b_k b_l I_{ijkl},$$

where the detector-efficiency-dependent integrals $I_{ijkl} \equiv \int \epsilon(\Omega')G_{ijkl}(\Omega')d\Omega'$ are independent of the fitting parameters $\mathcal{A}$. The integrals I_{ijkl} can be approximated by a Monte Carlo numerical integration technique. Using a large sample of phase space Monte Carlo events (Sec. IV C) generated uniformly in the five angles $(\cos\theta', \phi', \cos\theta_{\gamma\gamma'}, \cos\theta, \phi)$, we record whether each phase space MC event is reconstructed and passes the selection criteria. Using the known angular functions $G_{ijkl}(\Omega)$, we approximate the integral I_{ijkl} as

$$I_{ijkl} \equiv \int \epsilon(\Omega')G_{ijkl}(\Omega')d\Omega' \cong \frac{1}{N_{\rm phsp}} \sum_{p=1}^{N_{\rm phsp}} \Theta(p)G_{ijkl}(\Omega_p), \tag{26}$$

where $\Theta(p)$ is 1 (0) if the pth phase space event is (not) reconstructed and $N_{\rm phsp}$ is the total number of phase space events.

The most likely form of the parameters $\mathcal{A}$ given the PDF $F(\Omega;\mathcal{A})$ is found by maximizing the logarithm of the likelihood, which is given by Eq. (23) with the PDF F instead of W. The logarithm of the likelihood that the parameters $\mathcal{A}$ in the PDF $F(\Omega;\mathcal{A})$ describe the N_d data events occurring at angles Ω_d is

$$\log\mathcal{L}(\mathcal{A}) \equiv \log\prod_{d=1}^{N_d} F(\Omega_d;\mathcal{A}) = \sum_{d=1}^{N_d} \log F(\Omega_d;\mathcal{A})$$
$$= \sum_{d=1}^{N_d}\Big[\log\epsilon(\Omega_d) + \log W(\Omega_d;\mathcal{A})$$
$$- \log\sum_{ijkl} a_i a_j b_k b_l I_{ijkl}\Big]. \tag{27}$$

The first term in $\log\mathcal{L}$ is independent of the $\mathcal{A}$, so the log likelihood only depends on the detector efficiency through the phase space integrals. We reduce the number of parameters in the fit by recognizing that the multipole amplitudes are normalized (e.g., $a_1^2 + a_2^2 + a_3^2 = 1$). This method of performing an unbinned maximum likelihood over an angularly varying detector efficiency was first developed in Ref. [35]. The multidimensional optimization of $\log\mathcal{L}'(\mathcal{A})$ was achieved using the MINUIT MIGRAD variable-metric fitting routine [36].

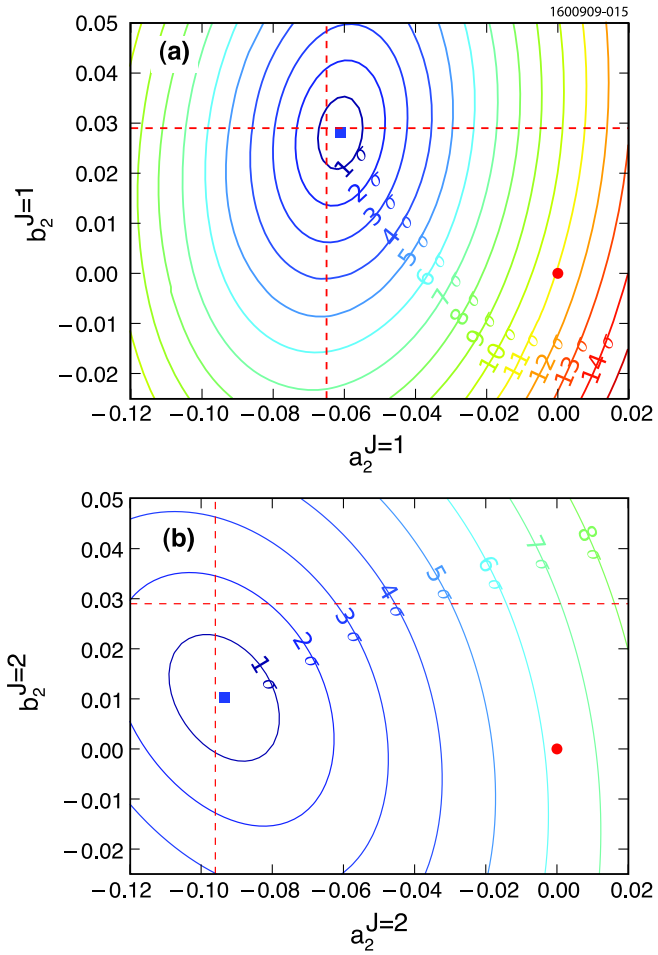

FIG. 5 (color online). (a) $J_\chi = 1$ and (b) $J_\chi = 2$ log likelihood contours as functions of (a_2, b_2) for two-parameter fits. The fitted values (the solid squares) are $(a_2, b_2) = (-0.0611, 0.0281)$ for $J_\chi = 1$ and $(a_2, b_2, a_3, b_3) = (-0.093, 0.010, 0, 0)$ for $J_\chi = 2$. These are, respectively, 11.1σ and 6.2σ from pure $E1$ (the solid circles). The theoretical values to first order in E_γ/m_c with $\kappa_c = 0$ are given by the dashed lines.

B. Statistical results of five-angle fits

1. $J_\chi = 1$ fits

The result of the two-parameter fit to the $J_\chi = 1$ data is $a_2^{J=1} = -0.0611 \pm 0.0063$, $b_2^{J=1} = 0.0281 \pm 0.0073$, based on 39 363 events. The efficiency integrals in the denominator were calculated by simulating 4.5×10^6 phase space MC events taking account of the detector geometry and selection criteria; 39.6% of events were reconstructed. Contours are shown in Fig. 5(a) of $\sqrt{2\Delta\log\mathcal{L}}$, where $\Delta\log\mathcal{L}$ is the difference in log likelihood between the fitted values of a_2, b_2, and any other values. For a pure $E1$ transition ($a_2 = b_2 = 0$) the value of $\chi_{E1} \equiv \sqrt{2\Delta\log\mathcal{L}}$ is 11.1.

The projections of the data in each of the five angles may be compared with curves based on a pure $E1$ distribution and on the fitted $M2/E1$ admixture. The angle θ is of

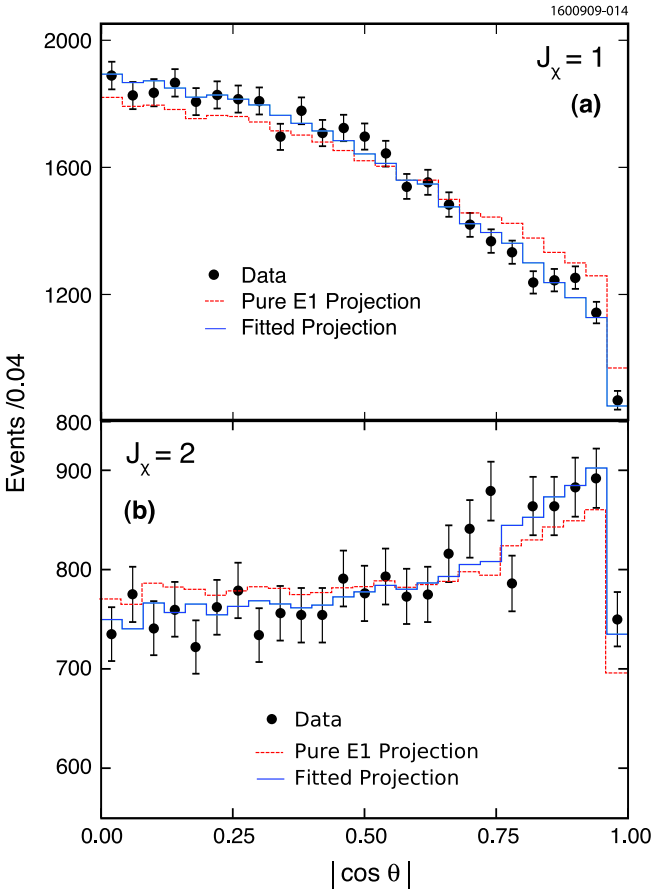

FIG. 6 (color online). (a) $J_\chi = 1$ and (b) $J_\chi = 2$ projections of $\cos\theta$ after using parity transformations to fold the data set into positive $\cos\theta'$, ϕ', $\cos\theta_{\gamma\gamma'}$, $\cos\theta$. For $J_\chi = 1$ ($J_\chi = 2$) the values of $\chi^2/N_{\text{d.o.f.}}$ for the 25 bin histogram describing the data to correspond with the two-parameter (a_2, b_2) fitted projection are $16.2/22 = 0.74$ ($20.3/22 = 0.92$) and to correspond with the pure $E1$ projection are $80.29/24 = 3.35$ ($35.5/24 = 1.48$). The fitted and pure $E1$ projections are selected from the same phase space MC sample (via the rejection method), resulting in the correlation of statistical fluctuations in the two projections.

particular importance as it is the angle that most clearly shows the preference of the data for an $M2/E1$ admixture over a pure $E1$ transition. The projection for $\cos\theta'$ also shows slightly better agreement with data with the fitted $M2/E1$ admixture than with a pure $E1$ transition. For the 50-bin histograms in $\cos\theta$, the reduced χ^2 $(\chi^2/N_{\text{d.o.f.}})^3$ comparing the data with the projection at the fitted values is $42.7/47 = 0.91$, while data and the pure $E1$ projection have a $\chi^2/N_{\text{d.o.f.}}$ of $108.5/49 = 2.21$.

Using the parity transformations described in Ref. [17], we can fold four of the five angles into the positive domain without modifying the value of the likelihood calculated through $W(\Omega; \mathcal{A})$. In Fig. 6(a) we show that the data are well matched with the projection in $|\cos\theta|$ with the fitted values of $\mathcal{A}$, but poorly matched with the pure-$E1$ $|\cos\theta|$ projection.

When we fix the ratio of the parameters to the theoretical ratio, given by Eq. (13), $a_2^{J=1}/b_2^{J=1} = -2.274$, we can perform a one-parameter fit to the five-angle $J_\chi = 1$ data set. The result of this one-parameter fit is $a_2^{J=1} = -0.0615 \pm 0.0055$, $b_2^{J=1} = -a_2^{J=1}/2.274 = 0.0271 \pm 0.0024$, with a value of $\chi_{E1} = \sqrt{2\Delta \log \mathcal{L}} = 11.1$) nearly identical to the results of the two-parameter fit. The results of these two fits are compared in Table III.

2. $J_\chi = 2$ fits

As the $J_\chi = 2$ PDF is parameterized by four multipole amplitudes (a_2, b_2, a_3, b_3), there are several choices of fits to be performed. The simplest would be a two-parameter fit with $a_3 = b_3 = 0$, as the $E3$ amplitudes should be zero in the absence of significant $S - D$ state mixing. For this type of fit to the 19 755 signal events, we find $a_2^{J=2} = -0.093 \pm 0.016$, $b_2^{J=2} = 0.010 \pm 0.013$ with these fit values favored by 6.2σ over a fit with pure $E1$.

Allowing for $S - D$ mixing in the ψ' state, the $b_3^{J=2}$ amplitude may be nonzero. When we perform a three-parameter fit (setting $a_3^{J=2} = 0$), we find $a_2^{J=2} = -0.093 \pm 0.016$, $b_2^{J=2} = 0.007 \pm 0.013$, $b_3^{J=2} = -0.008 \pm 0.011$, favored by 6.3σ over pure $E1$.

When we allow a nonzero $b_3^{J=2}$ amplitude, but fix the ratio of $a_2^{J=2}/b_2^{J=2} = -3.367$ by Eq. (15), we can perform a two-parameter fit that allows for $S - D$ mixing in the ψ' state. The results of this two-parameter fit are $a_2^{J=2} = -0.092 \pm 0.016$, $b_2^{J=2} = -a_2^{J=2}/3.367 = 0.027 \pm 0.005$, $b_3^{J=2} = -0.001 \pm 0.011$, favored by 6.1σ over pure $E1$.

When we perform the fit for the full four parameters (a_2, b_2, a_3, b_3), we find $a_2^{J=2} = -0.079 \pm 0.019$, $a_3^{J=2} = 0.002 \pm 0.014$, $b_2^{J=2} = 0.017 \pm 0.014$, $b_3^{J=2} = -0.008 \pm 0.012$, favored by 6.4σ over pure $E1$.

For the five-angle fit with two parameters, we plot the data with the pure $E1$ projection and the fitted value

TABLE III. $J_\chi = 1$ five-angle fit results. The fits were performed on 39363 events satisfying the selection criteria described in Sec. V. $\chi_{E1} \equiv \sqrt{2\Delta \log \mathcal{L}}$ is the number of standard deviations by which the fitted value differs from the pure $E1$ value.

Fit	$a_2^{J=1}$ (10^{-2})	$b_2^{J=1}$ (10^{-2})	χ_{E1}
Two-parameter	-6.11 ± 0.63	2.81 ± 0.73	11.1
One-parameter $(a_2/b_2 = -2.274)$	-6.15 ± 0.55	2.71 ± 0.24	11.1
Theory $(m_c = 1.5$ GeV)	$-6.5(1 + \kappa_c)$	$2.9(1 + \kappa_c)$	

TABLE IV. $J_\chi = 2$ five-angle fit results. The fits were performed on the 19755 signal events satisfying the selection criteria described in Sec. V. $\chi_{E1} \equiv \sqrt{2\Delta \log \mathcal{L}}$ is the number of standard deviations by which the fitted value differs from the pure $E1$ value.

Fit	$a_2^{J=2}$ (10^{-2})	$b_2^{J=2}$ (10^{-2})	$a_3^{J=2}$ (10^{-2})	$b_3^{J=2}$ (10^{-2})	χ_{E1}
Two-parameter	-9.3 ± 1.6	1.0 ± 1.3	0	0	6.2
Three-parameter	-9.3 ± 1.6	0.7 ± 1.3	0	-0.8 ± 1.2	6.3
Two-parameter ($b_2 = \frac{-a_2}{3.367}$)	-9.2 ± 1.6	2.7 ± 0.5	0	-0.1 ± 1.1	6.1
Four-parameter	-7.9 ± 1.9	0.2 ± 1.4	1.7 ± 1.4	-0.8 ± 1.2	6.4
Theory ($m_c = 1.5$ GeV)	$-9.6(1 + \kappa_c)$	$2.9(1 + \kappa_c)$	0	Model dep.	

projection of $|\cos\theta|$ in Fig. 6(b). As for $J_\chi = 1$, the fitted values match the data better than the pure $E1$ projection.

The results of the above fits are summarized in Table IV. In all cases there is at least 6.1σ evidence for multipoles beyond $E1$ in the transition $\psi' \to \gamma'\chi_{c2} \to \gamma'\gamma J/\psi$. The contours for $\sqrt{2\Delta \log \mathcal{L}}$ for a_2 vs b_2 for the two-parameter fits are shown in Fig. 5(b); the contours for all other pairs of variables for all the fits are Gaussian-shaped with a single local maximum.

VII. SYSTEMATIC UNCERTAINTIES

We now present the results of systematic studies for the fits to the five-angle distributions performed in the previous section. For $J_\chi = 1$, we perform all systematic studies on the two-parameter fit (a_2, b_2), as the one-parameter fixed-ratio fit produces nearly identical results. However, for $J_\chi = 2$, there are four types of five-angle fits:

(i) Two-parameter fit (a_2, b_2) with $a_3 \equiv b_3 \equiv 0$ (no $S - D$ or $P - F$ mixing),
(ii) Three-parameter fit (a_2, b_2, b_3) with $a_3 \equiv 0$, relevant for a D-wave admixture in the ψ',
(iii) Fixed-ratio two-parameter fit (a_2, b_3) with $b_2 \equiv -a_2/3.367$ and $a_3 \equiv 0$, and
(iv) Four-parameter fit (a_2, b_2, a_3, b_3).

In this paper, we describe in detail the systematic studies for the $J_\chi = 1$ case and the $J_\chi = 2$ case where $a_3 = b_3 \equiv 0$. Systematic studies for the other three $J_\chi = 2$ cases are discussed in detail in Ref. [37].

For many investigations into a possible systematic uncertainty, we perform an ensemble of fits on samples of signal events selected from a phase space data set via the rejection method to follow $W(\Omega; \mathcal{A}_0)$ for a given input set of multipole parameters. For each multipole a, we calculate the following parameters from the results of these ensembles of fits, with $N_{\rm ens}$ MC events in each member of the ensemble:

(i) $\langle a \rangle$, the mean of the fitted multipole amplitude over the ensemble of tests, with a statistical error corresponding to the variation of the fitted multipole amplitude over the ensemble of tests,
(ii) $\sigma_a^{\rm fit}$, the (mean of the) nominal uncertainty from each individual likelihood fit to multipole amplitude,
(iii) $\Delta_{\langle a \rangle}$, the deviation of the mean from the MC-generated value of the amplitude in units of the expected deviation of the mean $\sigma_{\langle a \rangle} = \sigma^{\rm fit}/\sqrt{N_{\rm ens}}$ defined as

$$\Delta_{\langle a \rangle} = \frac{\langle a \rangle - a^{\rm Input}}{\sigma_a^{\rm fit}/\sqrt{N_{\rm ens}}}, \quad \text{and} \tag{28}$$

(iv) $\Delta_{\sigma(a)}$, the deviation of the standard deviation when a potential systematic effect is present compared to the standard deviation without the effect being present (in units of the expected fluctuation the best estimate of the standard deviation from an ensemble of N measurements $\sigma_\sigma = \sigma/\sqrt{2N}$ ([10] Sec. 32.1.1), defined as

$$\Delta_{\sigma(a)} = \frac{\sigma^{\text{with syst}} - \sigma^{\text{without syst}}}{\sigma/\sqrt{2N_{\rm ens}}}. \tag{29}$$

For the $\sigma^{\rm fit}$ we list the mean of the nominal uncertainty, but for all tests performed the nominal uncertainty from every likelihood fit in the ensemble was essentially constant to the level of precision quoted.

For all of the systematic tests from ensembles of measurements, we assign a systematic uncertainty if either (a) we find that there is a significant bias $|\Delta_{\langle a \rangle}| > 1$ or if (b) there is an uncertainty that widens the ensemble distribution above the expected statistical fluctuation evidenced by $\Delta_{\sigma(a)} > 1$.

A. Toy MC check of fitting procedure

To test the accuracy of the fitting procedure described in Sec. VI A an ensemble of toy Monte Carlo fitting trials was performed. For each trial, we generated a large number of phase space events, where each event is described by five random numbers for each of the variables $(\cos\theta', \phi', \cos\theta_{\gamma\gamma'}, \cos\theta, \phi)$ uniformly distributed over their ranges.

We generated a set of toy signal Monte Carlo events by selecting events from a separate MC phase space data set

[3]The number of degrees of freedom $N_{\rm d.o.f.} = N_{\rm bins} - N_{\rm params} - 1$ where $N_{\rm bins}$ is the number of bins in the histogram, and $N_{\rm params}$ is the number of free parameters in the fit. The minus one accounts for the fact that the projections are normalized to contain the same number of events as the original data set.

via the rejection method, so the events are described by $W(\Omega;\mathcal{A}_0)$ for an input set of multipole parameters $\mathcal{A}_0$.

To test the $J_\chi = 1$ ($J_\chi = 2$) fits, we performed an ensemble of 200 toy MC trials in which each trial had $N_{\rm sig} = 40\,000$ (20 000) signal events after selection criteria were applied. We analytically calculated the phase space integrals, as the toy MC was thrown at 100% detector efficiency. In assigning the systematic uncertainty, we set the multipole amplitudes of the toy signal Monte Carlo to be $a_2^{J=1} = -0.065$, $b_2^{J=1} = 0.029$, ($a_2^{J=2} = -0.096$, $b_2^{J=2} = 0.029$, $a_3^{J=2} = 0$, $b_3^{J=2} = 0$) the expected value if $\kappa_c = 0$ to first order in E_γ/m_c. Fits with other values of input parameters recover the input results to similar precision. We find no systematic bias or uncertainty is associated with the fitting procedure described in this method, as the ensemble of trials is Gaussian-distributed with a width according to the statistical uncertainty.

B. Amount of phase space Monte Carlo needed for efficiency integrals

Using too few phase space Monte Carlo events would give poor approximations to the efficiency integrals, introducing an overall systematic uncertainty to the results of the maximum likelihood fit. We use 4.5×10^6 phase space events for the normalization, approximately 100 times the $J_\chi = 1$ data set (the larger of the two). By varying the size of the MC sample, we find no systematic uncertainty associated with any number of events exceeding 10^5, and hence assign no systematic error to this source.

C. Impurity systematic uncertainties

For the $J_\chi = 1$ ($J_\chi = 2$) selection criteria, approximately 0.23% (0.29%) of the events that pass the selection criteria are not signal events, but a background mode that must be considered for the possibility of introducing a systematic bias or uncertainty to our result. Taking our five-fold generic Monte Carlo data set and splitting it into five independent data sets, we find a purity and efficiency of 99.77% and 39.6% (99.71% and 36.0%). The main sources of impurity background modes for $J_\chi = 1$ are $\psi' \to \pi^0\pi^0 J/\psi$ and $\psi' \to \gamma'\chi_{c1}$ (where the χ_{c1} decay was not to $\gamma J/\psi$ followed by $J/\psi \to \ell^+\ell^-$). For $J_\chi = 2$ they are $\psi' \to \gamma'\chi_{c1}$ and $\psi' \to \pi^0\pi^0 J/\psi$.

For each of the five independent generic MC impurity backgrounds, we perform 31 (37) trials with and without the impurity background events present. For each trial, we replace the signal events originally present with phase space events selected via the rejection method to come up with many independent data sets. For each trial we perform one fit with no impurities present and one fit with the impurities. For a given set of impure background events, we find that the bias due to impurities varies very little between different trials. In Table V (Table VI), we list the difference from the fit with no impurities. For $J_\chi = 1$, we find a significant impurity bias that is relatively constant among all five sets of impure events, so we correct our fitted result for this impurity bias and assign a systematic uncertainty of half of the bias. For the $J_\chi = 2$ case, we find that the impurity bias significantly fluctuates between background data sets, so we assign a systematic uncertainty of the size of the fluctuation of the impurity bias.

D. Final state radiation

Another possible source of systematic uncertainty is the effect of final state radiation (FSR), which can alter the directions of the two leptons in the J/ψ rest frame affecting the variables $\cos\theta$ and ϕ. Generation of Monte Carlo samples has been done using EVTGEN, which models final state radiation in the decay sequences $J/\psi \to \ell^+\ell^-$ with PHOTOS. We estimate the effect of final state radiation by performing signal fits on the angles Ω from generator level four-vectors, both before and after final state radiation has been added. We use the rejection method to select events,

TABLE V. Generic MC tests for a systematic bias from impure events for $J_\chi = 1$. We split the five-fold generic MC data set into five data sets labeled (A)–(E), replacing the generic Monte Carlo signal events with events selected to obey $W(\Omega;\mathcal{A}_0)$ from the 4.5M event phase space MC data set. For each of these five data sets, we performed an ensemble of 31 fits. The difference rows show the shift in values of a_2 and b_2 comparing the individual fits before and after impurities are added. A positive shift means that to obtain the pure results we should subtract the bias from impurities. The set (A–E) is the result from adding all five data samples of impure events to a regular-sized set of signal events, and demonstrates how the impurities scale linearly in the $J_\chi = 1$ case.

Type	$\langle a_2\rangle$ (10^{-2})	$\langle\sigma^{\rm fit}_{a_2}\rangle$ (10^{-2})	$\Delta_{\langle a_2\rangle}$	$\langle b_2\rangle$ (10^{-2})	$\langle\sigma^{\rm fit}_{b_2}\rangle$ (10^{-2})	$\Delta_{\langle b_2\rangle}$
Pure	-6.54 ± 0.50	0.63	-0.32	2.97 ± 0.71	0.73	0.52
Difference w/impurities (A)	0.150 ± 0.002			0.058 ± 0.003		
Difference w/impurities (B)	0.120 ± 0.002			0.053 ± 0.003		
Difference w/impurities (C)	0.140 ± 0.003			0.060 ± 0.005		
Difference w/impurities (D)	0.216 ± 0.004			0.095 ± 0.005		
Difference w/impurities (E)	0.109 ± 0.002			-0.031 ± 0.003		
Difference w/impurities (A–E)	0.730 ± 0.011			0.241 ± 0.019		
Input	-6.50			2.90		
⟨Impurity bias⟩	0.15 ± 0.03			0.05 ± 0.03		

TABLE VI. Generic MC tests for a systematic bias from impure events for $J_\chi = 2$ for two-parameter (a_2, b_2) fit with $a_3 \equiv b_3 \equiv 0$. We find that the impurities add a negligible systematic uncertainty when compared with the statistical uncertainty.

Type	$\langle a_2 \rangle$ (10^{-2})	$\langle \sigma^{\rm fit}_{a_2} \rangle$ (10^{-2})	$\Delta_{\langle a_2 \rangle}$	$\langle b_2 \rangle$ (10^{-2})	$\langle \sigma^{\rm fit}_{b_2} \rangle$ (10^{-2})	$\Delta_{\langle b_2 \rangle}$
Pure	-9.8 ± 1.4	1.6	-0.6	3.0 ± 1.3	1.2	0.6
Difference w/impurities (A)	-0.005 ± 0.006			0.078 ± 0.003		
Difference w/impurities (B)	0.080 ± 0.004			-0.011 ± 0.005		
Difference w/impurities (C)	-0.008 ± 0.011			0.149 ± 0.004		
Difference w/impurities (D)	0.022 ± 0.003			-0.050 ± 0.003		
Difference w/impurities (E)	-0.041 ± 0.002			0.027 ± 0.003		
Difference w/impurities (A–E)	0.047 ± 0.019			0.190 ± 0.011		
Input	-9.6			2.9		
⟨Impurity Bias⟩	0.009 ± 0.040			0.038 ± 0.070		

so that the pre-FSR generator level four-vectors follow the PDF $W(\Omega; \mathcal{A}_0)$ for an input value of the multipole amplitudes $\mathcal{A}_0$. We also use the pre-FSR four-vectors when selecting the phase space events to be used as ''signal'' described by the PDF $W(\Omega; \mathcal{A}_0)$ with a given $\mathcal{A}_0 \equiv (a_2, b_2) = (-0.065, 0.029)$ (for $J_\chi = 2$, $\mathcal{A}_0 \equiv (a_2, b_2, a_3, b_3) = (-0.096, 0.029, 0.0, 0.0)$). We then compare the fit on the selected events using the pre-FSR and post-FSR generator level to check for a systematic uncertainty from final state radiation. Comparing $\Delta_{\sigma(a)}$ and $\Delta_{\langle a \rangle}$ for each multipole parameter for FSR, we find no statistically significant evidence for a systematic uncertainty due to FSR.

The angular distribution was also fit using data from $J/\psi \to e^+e^-$ and $J/\psi \to \mu^+\mu^-$ only, selected by the E/p selection criterion. Without correcting for possible systematic biases, we found the results in Table VII. Preliminary studies of simulated signal data (generated from phase space MC) indicated that the most accurate result is obtained by performing a fit to the combined $J/\psi \to \mu^+\mu^-$ and $J/\psi \to e^+e^-$ dataset, while still blinded to the actual dataset. The results from the fit to the muon-only dataset were similar to the results from the combined dataset. The electron-only dataset produces similar results to the fit results of the combined dataset, except for the χ_{c1} case where the two-parameter electron-only result deviates from the combined result by approximately 1.4σ. However, fixing the a_2/b_2 ratio reduces the deviation of the electron-only result to less than 1σ even in this worst case. Therefore, we assign no additional systematic uncertainty due to FSR from the results of the muon-only and electron-only fits.

E. Choice of kinematic fits

For our final analysis, we perform a 1C kinematic fit to the J/ψ mass and a 4C kinematic fit to the ψ' four momentum of the lab frame, and also perform bremsstrahlung reconstruction on each track if any showers were tagged as bremsstrahlung radiation belonging to the track. To test for possible systematic effects, we perform an ensemble of tests on phase space MC shaped to have $\mathcal{A}_0 = (-0.065, 0.029)$ for $J_\chi = 1$ and $\mathcal{A}_0 = (-0.096, 0.029, 0, 0)$ for $J_\chi = 2$ with four-vectors selected to have the pre-FSR generator photons follow $W(\Omega; \mathcal{A}_0)$. We construct the four-vectors for the variables in three ways: (1) Post-FSR generator level four-vectors; (2) 1C

TABLE VII. Fits to the angular distribution using only events where the J/ψ decays to two muons or two electrons. The χ_{c1} (χ_{c2}) dataset contained 20 968 (10 563) muon-only events and 18 395 (9192) electron-only events.

Fit	a_2 (10^{-2})	b_2 (10^{-2})	a_3 (10^{-2})	b_3 (10^{-2})
χ_{c1} Two-parameter $\mu\mu$	-7.23 ± 0.87	2.2 ± 1.0		
χ_{c1} Fixed-ratio $\mu\mu$	-6.85 ± 0.75	3.0 ± 0.3		
χ_{c1} Two-parameter ee	-4.85 ± 0.92	3.5 ± 1.0		
χ_{c1} Fixed-ratio ee	-5.36 ± 0.81	2.4 ± 0.4		
χ_{c2} Two-paramater $\mu\mu$	-8.1 ± 2.1	1.2 ± 1.7	0	0
χ_{c2} Three-parameter $\mu\mu$	-8.1 ± 2.1	1.1 ± 1.9	0	-0.3 ± 1.6
χ_{c2} Fixed-ratio $\mu\mu$	-8.1 ± 2.1	2.4 ± 0.6	0	0.2 ± 1.5
χ_{c2} Four-parameter $\mu\mu$	-5.4 ± 3.0	0.0 ± 2.0	3.6 ± 1.8	-0.2 ± 1.7
χ_{c2} Two-parameter ee	-10.7 ± 2.3	0.8 ± 1.8	0	0
χ_{c2} Three-parameter ee	-10.7 ± 2.3	0.2 ± 2.0	0	-1.4 ± 1.8
χ_{c2} Fixed-ratio ee	-10.5 ± 2.3	3.1 ± 0.7	0	-0.4 ± 1.6
χ_{c2} Four-parameter ee	-11.2 ± 3.0	0.4 ± 2.1	-0.6 ± 2.2	-1.4 ± 1.8

TABLE VIII. Results of data fits for $J_\chi = 1$ when applying various selection criteria. For all selection criteria considered, a systematic uncertainty is found of $(0.19, 0.22) \times 10^{-2}$ for (a_2, b_2), respectively, over the variation of the criteria.

Criteria	a_2^{biascor} (10^{-2})	b_2^{biascor} (10^{-2})
Default	$-6.26 \pm 0.63 \pm 0.15$	$2.76 \pm 0.73 \pm 0.06$
$E^{\text{3rd Shwr}} < 18$ MeV	$-6.43 \pm 0.64 \pm 0.08$	$2.67 \pm 0.73 \pm 0.06$
$E^{\text{3rd Shwr}} < 50$ MeV	$-5.73 \pm 0.60 \pm 0.30$	$2.45 \pm 0.72 \pm 0.13$
$\chi^2_{\text{k.f.}} < 10$	$-6.23 \pm 0.65 \pm 0.05$	$2.33 \pm 0.75 \pm 0.03$
$\chi^2_{\text{k.f.}} < 30$	$-6.30 \pm 0.61 \pm 0.32$	$3.10 \pm 0.71 \pm 0.04$
χ_c mass ± 10 MeV	$-6.36 \pm 0.65 \pm 0.11$	$2.85 \pm 0.75 \pm 0.04$
χ_c mass ± 20 MeV	$-6.10 \pm 0.62 \pm 0.18$	$2.78 \pm 0.69 \pm 0.09$
$\lvert\cos\theta^{\text{barrel}}_{\text{lab,ph}}\rvert < 0.77$	$-6.18 \pm 0.65 \pm 0.16$	$2.97 \pm 0.75 \pm 0.07$
$\lvert\cos\theta^{\text{barrel}}_{\text{lab,ph}}\rvert < 0.80$	$-6.17 \pm 0.62 \pm 0.16$	$2.73 \pm 0.72 \pm 0.07$
Ensemble	-6.20 ± 0.19	2.74 ± 0.22

TABLE IX. Results of data fits when applying various selection criteria to $J_\chi = 2$ two-parameter (a_2, b_2) fits $(a_3 \equiv b_3 \equiv 0)$. For all sets of criteria, a systematic uncertainty is found of $(0.3, 0.3) \times 10^{-2}$ for (a_2, b_2), respectively, over the variation of the criteria.

Criteria	a_2 (10^{-2})	b_2 (10^{-2})
Default	-9.3 ± 1.6	1.0 ± 1.3
$E^{\text{3rd Shwr}} < 18$ MeV	-9.4 ± 1.6	0.6 ± 1.3
$E^{\text{3rd Shwr}} < 50$ MeV	-9.8 ± 1.6	0.5 ± 1.3
$\chi^2_{\text{k.f.}} < 10$	-9.1 ± 1.6	1.3 ± 1.3
$\chi^2_{\text{k.f.}} < 30$	-9.5 ± 1.5	0.4 ± 1.2
χ_c mass ± 10 MeV	-8.7 ± 1.6	1.0 ± 1.3
χ_c mass ± 20 MeV	-9.8 ± 1.5	0.8 ± 1.3
$\lvert\cos\theta^{\text{barrel}}_{\text{lab,ph}}\rvert < 0.77$	-9.6 ± 1.6	1.2 ± 1.3
$\lvert\cos\theta^{\text{barrel}}_{\text{lab,ph}}\rvert < 0.80$	-9.5 ± 1.5	1.3 ± 1.3
Ensemble	-9.4 ± 0.3	0.9 ± 0.3

and 4C kinematic fits without bremsstrahlung recovery; (3) 1C and 4C kinematic fits with bremsstrahlung recovery. For each four-vector type, we perform as many fits as possible using a data size (after selection criteria) of 40 000 $J_\chi = 1$ (20 000 $J_\chi = 2$) events in each fit. We find no statistically significant systematic effect from this procedure.

F. Variation of selection criteria

To look for an additional systematic uncertainty from possible variations of selection criteria, we looked at effects of the following variations on statistical and systematic impurity uncertainties: maximum third shower energy, maximum reduced χ^2, χ_c mass window, and maximum cosine of polar angle for photons in the barrel region. Variations were explored which loosened and tightened all our selection criteria. For $J_\chi = 1$ we found that the default criteria (defined in Sec. V) had the smallest quadrature sum of the statistical uncertainty with impurity systematic uncertainty. We further found that over the ensemble of tests involving various criteria, the mean from the ensemble of tests for a_2 and b_2 (when no impurities were present) varied only slightly. For the $J_\chi = 2$ two-parameter (a_2, b_2) fit case, we found that while we were quite near the minimal total quadrature sum for the default criteria, we could have achieved a $\sim 3\%$ improvement if we loosened these conditions. However, to achieve that $\sim 3\%$ improvement requires increasing the number of impure events by a factor of approximately five as shown in Fig. 3, so this was not performed.

After looking at the effect of variations of selection criteria on an ensemble of tests using the "signal" data selected from phase space MC via the rejection method, we looked at the actual effect of performing fits to data after applying various criteria. These results show the sensitivity of the data to the chosen criteria. For the $J_\chi = 1$ case shown in Table VIII, we perform the fits using the various criteria, and then correct for the impurity bias. We then consider the ensemble of bias-corrected data fits and assign a systematic uncertainty using the standard deviation of the fitted results over the 7 types of criteria considered. We find a systematic uncertainty of $(0.19, 0.22) \times 10^{-2}$ for $(a_2^{J=1}, b_2^{J=1})$ in performing fits to data.

For $J_\chi = 2$ (Table IX), we follow a similar procedure but do not correct for impurity biases before calculating the systematic uncertainty, as the impurity bias in all cases is less than 1/10 the statistical uncertainty, so any correction would be of very little significance. We find in this case systematic uncertainties of $(0.3, 0.3) \times 10^{-2}$ for (a_2, b_2) when performing the two-parameter fit with $(a_3 \equiv b_3 \equiv 0)$.

TABLE X. Systematic uncertainties and biases for $J_\chi = 1$. The total systematic error is the quadrature sum of systematic uncertainties and the signed sum of systematic biases. The statistical uncertainty from the data fits is given for comparison.

Systematic uncertainty	$a_2^{J=1}$		$b_2^{J=1}$	
	Uncertainty (10^{-2})	Bias (10^{-2})	Uncertainty (10^{-2})	Bias (10^{-2})
Generic MC impurities	0.15	0.15	0.05	0.05
Selection criteria	0.19	-	0.22	-
Total systematic uncert.	0.24	0.15	0.23	0.05
Statistical uncertainty	0.63	-	0.73	-

TABLE XI. Systematic uncertainties for $J_\chi = 2$ two-parameter fit with a_2, b_2.

Systematic uncertainty	$a_2^{J=2}$ (10^{-2})	$b_2^{J=2}$ (10^{-2})
Generic MC impurities	0.04	0.07
Selection criteria	0.33	0.33
Total systematic uncertainty	0.3	0.3
Statistical uncertainty	1.6	1.3

TABLE XII. Systematic uncertainties for $J_\chi = 2$ three-parameter fit for a_2, b_2, b_3.

Systematic uncertainty	$a_2^{J=2}$ (10^{-2})	$b_2^{J=2}$ (10^{-2})	$b_3^{J=2}$ (10^{-2})
Generic MC impurities	0.04	0.07	0.03
Selection criteria	0.33	0.34	0.20
Total systematic uncertainty	0.3	0.3	0.2
Statistical uncertainty	1.6	1.4	1.2

TABLE XIII. Systematic uncertainties for $J_\chi = 2$ two-parameter fit for a_2, b_3 with fixed values of $b_2 \equiv -a_2/3.367$ and $a_3 \equiv 0$.

Systematic uncertainty	$a_2^{J=2}$ (10^{-2})	$b_3^{J=2}$ (10^{-2})
Generic MC impurities	0.04	0.04
Selection criteria	0.34	0.23
Total systematic uncertainty	0.3	0.2
Statistical uncertainty	1.6	1.1

G. Summary of systematic uncertainties and biases

The systematic uncertainties and biases for $J_\chi = 1$ are summarized in Table X. We find the total systematic uncertainty to be $(0.24, 0.23) \times 10^{-2}$ for $(a_2^{J=1}, b_2^{J=1})$, respectively. The systematic uncertainties for the $J_\chi = 2$ two-parameter fit (a_2, b_2) are summarized in Table XI, and for other fits in Tables XII, XIII, and XIV. In each case the total systematic error is the quadrature sum of systematic uncertainties, and the statistical uncertainty for the data fits is given for comparison. We do not find any systematic biases for the $J_\chi = 2$ case.

VIII. CONCLUSIONS

A. Normalized multipole amplitudes

The results of our bias-corrected fits with systematic uncertainties for $J_\chi = 1$ with the two-parameter fit are

$$a_2^{J=1} = (-6.26 \pm 0.63 \pm 0.24) \times 10^{-2}, \quad (30)$$

$$b_2^{J=1} = (2.76 \pm 0.73 \pm 0.23) \times 10^{-2}. \quad (31)$$

The results of our fits with systematic uncertainties for $J_\chi = 2$ with the two-parameter fit (a_2, b_2) with $a_3 = b_3 \equiv 0$ are

$$a_2^{J=2} = (-9.3 \pm 1.6 \pm 0.3) \times 10^{-2}, \quad (32)$$

$$b_2^{J=2} = (1.0 \pm 1.3 \pm 0.3) \times 10^{-2}; \quad (33)$$

for the three-parameter fit (a_2, b_2, b_3) with $a_3 \equiv 0$:

$$a_2^{J=2} = (-9.3 \pm 1.6 \pm 0.3) \times 10^{-2}, \quad (34)$$

$$b_2^{J=2} = (0.7 \pm 1.4 \pm 0.3) \times 10^{-2}, \quad (35)$$

$$b_3^{J=2} = (-0.8 \pm 1.2 \pm 0.2) \times 10^{-2}; \quad (36)$$

for the two-parameter fit (a_2, b_3) with fixed values of $b_2 \equiv -a_2/3.367$ and $a_3 \equiv 0$:

$$a_2^{J=2} = (-9.2 \pm 1.6 \pm 0.3) \times 10^{-2}, \quad (37)$$

$$b_2^{J=2} \equiv -\frac{a_2^{J=2}}{3.367} = (2.7 \pm 0.5 \pm 0.1) \times 10^{-2}, \quad (38)$$

$$b_3^{J=2} = (-0.1 \pm 1.1 \pm 0.2) \times 10^{-2}; \quad (39)$$

and for the four-parameter fit (a_2, b_2, a_3, b_3):

$$a_2^{J=2} = (-7.9 \pm 1.9 \pm 0.3) \times 10^{-2}, \quad (40)$$

$$b_2^{J=2} = (0.2 \pm 1.5 \pm 0.4) \times 10^{-2}, \quad (41)$$

$$a_3^{J=2} = (1.7 \pm 1.4 \pm 0.3) \times 10^{-2}, \quad (42)$$

$$b_3^{J=2} = (-0.8 \pm 1.2 \pm 0.2) \times 10^{-2}. \quad (43)$$

Our results are compared with previous experiments and theory in Fig. 7. The $J_\chi = 2$ results shown are for the two-parameter fit with $a_3 = b_3 = 0$.

B. Ratios independent of m_c and κ_c

Using the results from the $J_\chi = 2$ two-parameter (a_2, b_2) fit and the $J_\chi = 1$ fit, we find the ratios with the highest statistical sensitivity compare very well with the theoretical predictions:

TABLE XIV. Systematic uncertainties for $J_\chi = 2$ four-parameter fit with a_2, b_2, a_3, b_3.

Systematic uncertainty	$a_2^{J=2}$ (10^{-2})	$b_2^{J=2}$ (10^{-2})	$a_3^{J=2}$ (10^{-2})	$b_3^{J=2}$ (10^{-2})
Generic MC impurities	0.06	0.08	0.08	0.03
Selection criteria	0.24	0.39	0.28	0.20
Total systematic uncertainty	0.3	0.4	0.3	0.2
Statistical uncertainty	1.9	1.5	1.4	1.2

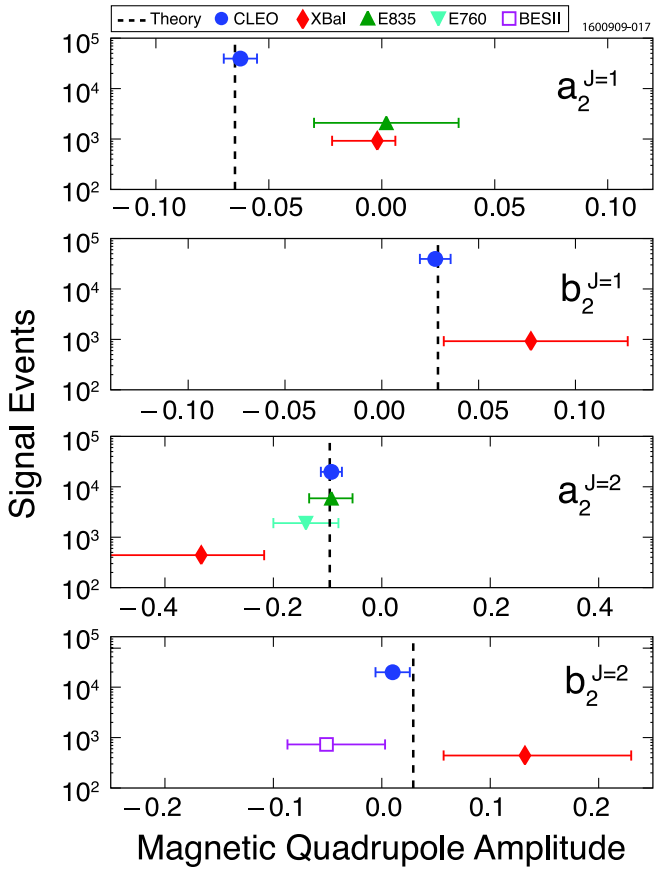

FIG. 7 (color online). Experimental values of the magnetic quadrupole amplitudes from this analysis compared with previous experimental values and theoretical expectations. For $J_\chi = 2$, results are shown for the two-parameter fit. CLEO-c results from this analysis are solid circles; Crystal Ball results are diamonds [17], the E760 result is a ∇ [18], the E835 results are $\triangle$'s [12], the BESII result is an open square [19], and the theoretical expectations given by Eqs. (7)–(10) with $m_c = 1.5$ GeV and $\kappa_c = 0$ are dashed lines.

$$\left(\frac{a_2^{J=1}}{a_2^{J=2}}\right)_{\mathrm{CLEO}} = 0.67^{+0.19}_{-0.13} \stackrel{?}{=} \left(\frac{a_2^{J=1}}{a_2^{J=2}}\right)_{\mathrm{th}} = 0.676 \pm 0.071, \tag{44}$$

$$\left(\frac{a_2^{J=1}}{b_2^{J=1}}\right)_{\mathrm{CLEO}} = -2.27^{+0.57}_{-0.99} \stackrel{?}{=} \left(\frac{a_2^{J=1}}{b_2^{J=1}}\right)_{\mathrm{th}} = -2.27 \pm 0.16, \tag{45}$$

$$\left(\frac{b_2^{J=2}}{b_2^{J=1}}\right)_{\mathrm{CLEO}} = 0.37^{+0.53}_{-0.47} \stackrel{?}{=} \left(\frac{b_2^{J=2}}{b_2^{J=1}}\right)_{\mathrm{th}} = 1.000 \pm 0.015, \tag{46}$$

$$\left(\frac{b_2^{J=2}}{a_2^{J=2}}\right)_{\mathrm{CLEO}} = -0.11^{+0.14}_{-0.15} \stackrel{?}{=} \left(\frac{b_2^{J=2}}{a_2^{J=2}}\right)_{\mathrm{th}} = -0.297 \pm 0.025. \tag{47}$$

C. κ_c calculation

Our most sensitive measurement of a magnetic quadrupole amplitude is that of $a_2^{J=1}$. From theory, we know that

$$a_2^{J=1} = -\frac{E_\gamma}{4m_c}(1 + \kappa_c) = (1 + \kappa_c)/\xi, \tag{48}$$

where we defined $1/\xi$ to be the proportionality between $1 + \kappa_c$ and $a_2^{J=1}$. If we use $m_c = (1.5 \pm 0.3)$ GeV, we find $\xi \equiv -(4m_c)/E_\gamma = -14.0 \pm 2.8$, so

$$1 + \kappa_c = \xi a_2^{J=1} = 0.877 \pm 0.088 \pm 0.034 \pm 0.175, \tag{49}$$

where we list the result, the statistical uncertainty, the systematic uncertainty, and the theoretical uncertainty from $m_c = 1.5 \pm 0.3$ GeV.

D. Summary

We measure significant nonzero magnetic quadrupole amplitudes for the transitions $\chi_{c1} \to \gamma J/\psi$, $\chi_{c2} \to \gamma J/\psi$, and $\psi' \to \gamma' \chi_{c1}$. Our fits to these three amplitudes all agree well with the theoretical predictions to first order in the ratio of photon energy to charmed quark mass with $\kappa_c = 0$ and $m_c = 1.5$ GeV. The data are consistent with the lattice QCD prediction (16) for $\chi_{c1} \to \gamma J/\psi$), but not with that for $\chi_{c2} \to \gamma J/\psi$ [15]. For the transition $\psi' \to \gamma' \chi_{c2}$, we do not measure a significant $M2$ amplitude, though this case has the largest uncertainty since there are fewer $J_\chi = 2$ signal events and $E_{\gamma'} < E_\gamma$ so $|b_2| < |a_2|$. The nonzero $M2$ amplitude in the transitions $\chi_{(c1,c2)} \to \gamma J/\psi$ is evident when comparing the $\cos\theta$ histograms for the data with the histograms for phase-space-Monte Carlo events selected to have a pure $E1$ distribution and the fitted values of the multipole amplitudes (as shown in Fig. 6). We find that for the $J_\chi = 1$ and $J_\chi = 2$ transitions our fitted results differ from the pure $E1$ value by more than 11σ and 6σ, respectively.

The agreement between data and theory is in stark contrast in some cases to previous measurements. With about 20 times the largest previous data sample, and a more sophisticated detector, the matter now seems to be resolved.

ACKNOWLEDGMENTS

We gratefully acknowledge the effort of the CESR staff in providing us with excellent luminosity and running conditions. D. Cronin-Hennessy thanks the A.P. Sloan Foundation. J. Rosner thanks the Aspen Center for Physics for hospitality. This work was supported by the National Science Foundation, the U.S. Department of Energy, the Natural Sciences and Engineering Research Council of Canada, and the U.K. Science and Technology Facilities Council.

[1] G. Karl, S. Meshkov, and J. L. Rosner, Phys. Rev. D **13**, 1203 (1976).
[2] G. Karl, S. Meshkov, and J. L. Rosner, Phys. Rev. Lett. **45**, 215 (1980).
[3] J. L. Rosner, Phys. Rev. D **78**, 114011 (2008).
[4] L. S. Brown and R. N. Cahn, Phys. Rev. D **13**, 1195 (1976).
[5] M. G. Olsson, C. J. Suchyta, A. D. Martin, and W. J. Stirling, Phys. Rev. D **31**, 1759 (1985).
[6] N. Brambilla *et al.* (Quarkonium Working Group), CERN Report No. CERN-2005-005, 2004.
[7] J. L. Rosner, Phys. Rev. D **64**, 094002 (2001).
[8] J. L. Rosner, Ann. Phys. (N.Y.) **319**, 1 (2005).
[9] J. D. Richman, California Institute of Technology Report No. CALT-68-1148, 1984.
[10] C. Amsler *et al.* (Particle Data Group), Phys. Lett. B **667**, 1 (2008).
[11] K. J. Sebastian, H. Grotch, and F. L. Ridener, Phys. Rev. D **45**, 3163 (1992).
[12] M. Ambrogiani *et al.* (E835 Collaboration), Phys. Rev. D **65**, 052002 (2002).
[13] R. McClary and N. Byers, Phys. Rev. D **28**, 1692 (1983).
[14] J. J. Dudek, R. G. Edwards, and D. G. Richards, Phys. Rev. D **73**, 074507 (2006).
[15] J. Dudek, R. Edwards, and C. Thomas, Phys. Rev. D **79**, 094504 (2009).
[16] M. Oreglia, Ph.D. thesis, Stanford [SLAC Report No. SLAC-0236, 1980].
[17] M. Oreglia *et al.* (Crystal Ball Collaboration), Phys. Rev. D **25**, 2259 (1982).
[18] T. Armstrong *et al.* (E760 Collaboration), Phys. Rev. D **48**, 3037 (1993).
[19] M. Ablikim *et al.* (BES Collaboration), Phys. Rev. D **70**, 092004 (2004).
[20] Y. Kubota *et al.* (CLEO Collaboration), Nucl. Instrum. Methods Phys. Res., Sect. A **320**, 66 (1992).
[21] D. Peterson *et al.*, Nucl. Instrum. Methods Phys. Res., Sect. A **478**, 142 (2002).
[22] H. Mendez *et al.* (CLEO Collaboration), Phys. Rev. D **78**, 011102 (2008).
[23] D. J. Lange, Nucl. Instrum. Methods Phys. Res., Sect. A **462**, 152 (2001).
[24] E. Barberio and Z. Was, Comput. Phys. Commun. **79**, 291 (1994).
[25] J. Z. Bai *et al.* (BES Collaboration), Phys. Rev. Lett. **88**, 101802 (2002).
[26] S. B. Athar *et al.* (CLEO Collaboration), Phys. Rev. D **70**, 112002 (2004).
[27] T. K. Pedlar *et al.* (CLEO Collaboration), Phys. Rev. D **72**, 051108 (2005).
[28] G. S. Adams *et al.* (CLEO Collaboration), Phys. Rev. Lett. **101**, 101801 (2008).
[29] P. Naik *et al.* (CLEO Collaboration), Phys. Rev. D **78**, 031101 (2008).
[30] K. M. Ecklund *et al.* (CLEO Collaboration), Phys. Rev. D **78**, 091501 (2008).
[31] Q. He *et al.* (CLEO Collaboration), Phys. Rev. D **78**, 092004 (2008).
[32] R. E. Mitchell *et al.* (CLEO Collaboration), Phys. Rev. Lett. **102**, 011801 (2009).
[33] D. M. Asner *et al.* (CLEO Collaboration), Phys. Rev. D **79**, 072007 (2009).
[34] T. Sjostrand *et al.*, Comput. Phys. Commun. **135**, 238 (2001).
[35] D. Cassel *et al.*, Phys. Rev. D **24**, 2787 (1981).
[36] F. James and M. Roos, Comput. Phys. Commun. **10**, 343 (1975).
[37] J. Ledoux, Ph.D. thesis, Cornell University, 2009.